Engineering Structures 200 (2019) 109719

Contents lists available at ScienceDirect

Engineering Structures

journal homepage: www.elsevier.com/locate/engstruct

Static load test on progressive collapse resistance of fully assembled precast concrete frame structure

Yun Zhou[a,b,c], Taiping Chen[c], Yilin Pei[c], Hyeon-Jong Hwang[c,*], Xiang Hu[c], Weijian Yi[a,c], Lu Deng[a,c]

[a] Hunan Provincial Key Lab on Damage Diagnosis for Engineering Structures, College of Civil Engineering, Hunan University, Changsha, Hunan 410082, China
[b] Key Laboratory for Green & Advanced Civil Engineering Materials and Application Technology of Hunan Province, College of Civil Engineering, Hunan University, Changsha, Hunan 410082, China
[c] College of Civil Engineering, Hunan University, Changsha 410082, China

ARTICLE INFO

Keywords:
Progressive collapse
PC moment frame
Beam-column joint
Dowel bar
Column removal
Finite element analysis

ABSTRACT

The progressive collapse behavior of fully assembled PC structures using dry connections under explosion, uncontrolled fire, and vehicle impact loads has seldom been studied. In the present study, three half scale moment sub-structures including a conventional RC specimen and two PC specimens using dowel bars and corbel were tested to investigate the progressive collapse performance. Collapse of the moment frame specimens with two spans was generated by the mid-column removal scenario under static loading. The test result showed that the peak strength of the PC specimens was only 76–81% of that of the RC specimen in compressive arch action and the ultimate displacement of the mid-column was 72–77% of that of the RC specimen. Unlike the RC specimen, catenary action was not completely developed in the PC specimens showing lower ductility. The load-displacement relationship and failure modes of the specimens agreed well with the prediction by finite element analysis, and a parametric study was conducted addressing various connection details to improve the progressive collapse performance of the PC moment sub-structure.

1. Introduction

Under progressive collapse of structures, local damage due to occasional and abnormal events such as gas explosions, vehicle impact, and uncontrolled fire exceeds the allowable resistance of the structural system, which increases a final damage that is disproportionate to the initial local damage [1–3]. Since Ronan Point apartment in London collapsed in 1968, the progressive collapse resistance of multi-story structures has been widely studied. Relevant design approaches were generally proposed to reduce the risk of initial damage and to arrest disproportionate propagations of a local failure [4]. Progressive collapse of the Alfred Murrah Federal Building and the Twin Towers of World Trade Centre due to terrorist attacks gave further impetus to the issuance of design codes and guidelines for building structures against abnormal loading conditions [5]. Recently, precast concrete (PC) structures are popular due to effective control in material quality and workmanship in large construction sites. To improve the constructability, dry connections such as the welding connection, bolted connection, and angle cleat plates are preferred in fully assembled PC moment frames [6–8]. However, because various PC joints without enough continuous reinforcement have obviously low structural integrity, the progressive collapse performance of PC structures may be lower than that of reinforced concrete (RC) structures.

Current design codes including GSA [9] and DoD [10] prescribe an alternate load path method to consider the potential of progressive collapse in design of multi-story buildings. For the overall structural integrity, the minimum continuous reinforcement should be used in beam-column joints [11]. In moment frames under progressive collapse, the structural performance is developed by compressive arch action (CAA) and catenary action (CTA). In CAA, flexural moment capacity of beams is increased by the horizontally restrained boundaries. When the deflection exceeds one beam depth after the peak strength, CTA provides the additional load-carrying capacity and deformation capacity due to tension force of beam longitudinal bars [12].

Recently, various researchers have studied the progressive collapse performance of PC structures. Nimse et al. [13,14] performed the progressive collapse test for one-third scale PC moment frames using field-bolted connections, and compared with the structural

* Corresponding author.
E-mail addresses: zhouyun05@hnu.edu.cn (Y. Zhou), hnu_chentp2015@163.com (T. Chen), yilin_pei@hnu.edu.cn (Y. Pei), hwanggun85@naver.com (H.-J. Hwang), baren@hnu.edu.cn (X. Hu), wjyi@hnu.edu.cn (W. Yi), denglu@hnu.edu.cn (L. Deng).

https://doi.org/10.1016/j.engstruct.2019.109719
Received 31 December 2018; Received in revised form 4 September 2019; Accepted 25 September 2019

performance of RC moment frames. Tohidi et al. [15] studied the applicability of the tensile tie force method to PC cross wall buildings for the progressive collapse analysis in *ABAQUS* program. Main et al. [16] carried out the test and analysis to investigate the structural behavior and failure modes of two PC moment frames where steel angles embedded in beams and columns were weld-connected by steel link plates. Kang and Tan [17] tested five half scale PC moment frames using various rebar details in cast-in-place connections under a column removal scenario. Klasila [18] performed the dynamic numerical analysis in a fully assembled PC building when a corner column lost the load-carrying capacity. Kang and Tan [19] evaluated the effects of 90° hook and lap-splice of the beam bottom bars in the joint on the progressive collapse performance of four PC moment sub-structures under quasi-static loading. Elsanadedy et al. [20] used *LS-DYNA* program for nonlinear numerical analysis to predict the structural performance of non-prestressed PC beam-column joints. Qian and Li [21] investigated the effect of connection types on the progressive collapse of a one-third scale RC beam-slab sub-structure and two one-third scale PC sub-structures with the welded- and pinned-connections. Feng et al. [22] considered the beam bar-slip at the beam-column joint to simulate the progressive collapse behavior of the PC sub-assemblages in *OpenSees* program, and reported that the bar-slip decreased the load-carrying capacity of CAA and increased the rotation capacity of the beam ends. Lin et al. [23] proposed a novel Multi-Hazard Resistant Prefabricated Concrete (MHRPC) frame system to satisfy both the seismic and progressive collapse design requirements. The proposed fame system exhibited the characteristics of large rotation, low damage, self-centering, and ease of repair under cyclic and progressive collapse behavior. Spencer et al. [24] proposed a new spandrel-to-column moment connection that utilized the unbonded high-strength steel post-tensioning bars passing through ducts of a column and anchored to spandrels via bearing plates. Full-scale quasi-static pushdown test results showed that the connection satisfied the design yield capacity and moderate-to-high ductility. Bournas et al. [25] conducted the pseudo-dynamic load tests on a full-scale 3-storey PC building, in which the slab-beam system was assembled with the dry mechanical connections. Kataoka et al. [26] performed the numerical analysis to investigate the effects of continuity bar diameter and cast in place concrete on the load-carrying capacity of PC beam-slab structures with dowel bar connections. Ren et al. [27] and Lu et al. [28] studied the progressive collapse resistance of beam-slab sub-structures. Qian et al. [29] evaluated the dynamic load redistribution of multi-panel RC flat-slab structures subjected to one-column or two-column removal scenario, and reported that the RC slab contributed to load redistribution and punching shear failure was not occurred in the slab-column connections with drop panels. Qian et al. [30] investigated the effect of connection types on the progressive collapse resistance of PC structures using a special link between the PC slab and PC beam. Qian et al. [31] reported that the PC beams and slab systems could provide substantial CAA, and the load-carrying capacity under large deformation was mainly attributed to CTA developed in the PC beams. With the development of assembled buildings, the progressive collapse performance of PC structures has been concerned by engineers because various PC joints having less continuous reinforcement exhibit obviously low structural integrity. Although the progressive collapse performance of PC moment frames using wet connection has been widely studied, the structural performance of fully assembled PC moment frames using dry connection was comparatively less discussed. Further, few design codes and guidelines can be applied to PC structures.

The present study focused on the progressive collapse performance of the fully assembled PC structure with dry connection. To investigate the effect of dry connection on PC structures, static loading tests and finite element analysis (FEA) were performed on a half scale RC and two half scale PC moment sub-structures where the mid-column removal scenario was simulated. The progressive collapse performance including the load transfer mechanism, deformation capacity, rebar strain, crack distribution, and failure modes were evaluated. FEA predicted well the test results, and a parametric study was conducted by using various design parameters, to further improve the progressive collapse performance of PC moment sub-structures.

2. Test program

2.1. Test specimens

To study the progressive collapse performance of fully assembled PC moment frame structures, a four-span 7-story moment frame structure used as residential building was designed according to *Code for Design of Concrete Structures* [32] and *Code for Seismic Design of Buildings* [33]. Floor height was 3.6 m, and span was 6 m and 7.5 m in the x- and y-directions, respectively. 5.0 kN/m^2 and 2.0 kN/m^2 were considered for design dead and live loads, respectively. Seismic intensity was classified as degree 7, and the design basic earthquake acceleration T_g was defined as 0.1 g according to Chinese design code GB 50011-2010 [33]. The field category was defined as class 2, which refers the field with a mean shear wave velocity V_{30} between 260 m/s and 510 m/s in US code [34]. An interior moment sub-frame was considered as a test specimen to investigate the load transfer path and failure mechanism under the removal of the mid-column by accidental loads. The specimen design was based on the three-dimensional analysis results using *SATWE* modular in *PKPM* program. Considering a semi-rigid boundary condition of the actual PC joint, the maximum moment in both cases of the fully fixed and hinged boundary conditions was used in the specimen design. Fig. 1 and Table 1 show the details and test parameters of a RC moment frame and two PC moment frames for static progressive collapse test. The specimens consist of two span beams and three columns with a removed mid-column. The cross section of the beam was 200 mm × 300 mm. The cross section and height of the column were 350 mm × 350 mm and 3000 mm, respectively. The test parameters were the assemblage methods (i.e., RC or PC), and corbel location in the fully assembled PC specimens (i.e., exposed corbel in specimen PC1 or hidden corbel in specimen PC2). The connection details of the PC specimens were determined according to design guideline of PC structures [7,32].

For specimen RC, four T18 bars (diameter = 18 mm and cross-sectional area = 254.5 mm^2) and eight T16 bars (diameter = 16 mm and cross-sectional area = 201.1 mm^2) were used for longitudinal bars of the beam and column, respectively. R6 bar (diameter = 6 mm and cross-sectional area = 28.3 mm^2) was used for transverse reinforcement at a spacing of 50 mm in the plastic hinge region of the beam and column. In the beam-column joint, R6 bar was placed at a spacing of 40 mm. A conventional connection method was used in the beam-column joint. For specimen PC1, PC beams and columns were separately prefabricated. The PC beams were connected with the PC columns by using dowel bars and steel angle cleat. The dowel bars were embedded in a prefabricated corbel of the PC column, and the prefabricated PC beams were lifted up and placed into the specific location to connect both sides of the column, in which the dowel bars embedded from the corbel were penetrated throughout the reserved holes at the PC beam end. Two dowel bars with 20 mm diameter projected from a corbel of the PC column were inserted into two dowel sleeve holes with 40 mm diameter embedded in the PC beam end. The diameter of the dowel bar was determined to resist horizontal shear force. The steel angle cleat stiffened with three side plates was installed on the top face of the PC beam end to further improve the load transfer capacity, on the basis of existing studies using the steel angle cleat without side plates [35]. The top of the dowel bars was bolt-connected with the steel angle cleat, and the high-strength bolts passing through the PC column were used to fix the steel angle cleat. The gap and holes of the specimen were filled by non-shrink high-strength grouting material. Horizontal U-shaped bars were used in the PC beam ends and corbels to prevent local failure of concrete and to improve the dowel bar performance. For

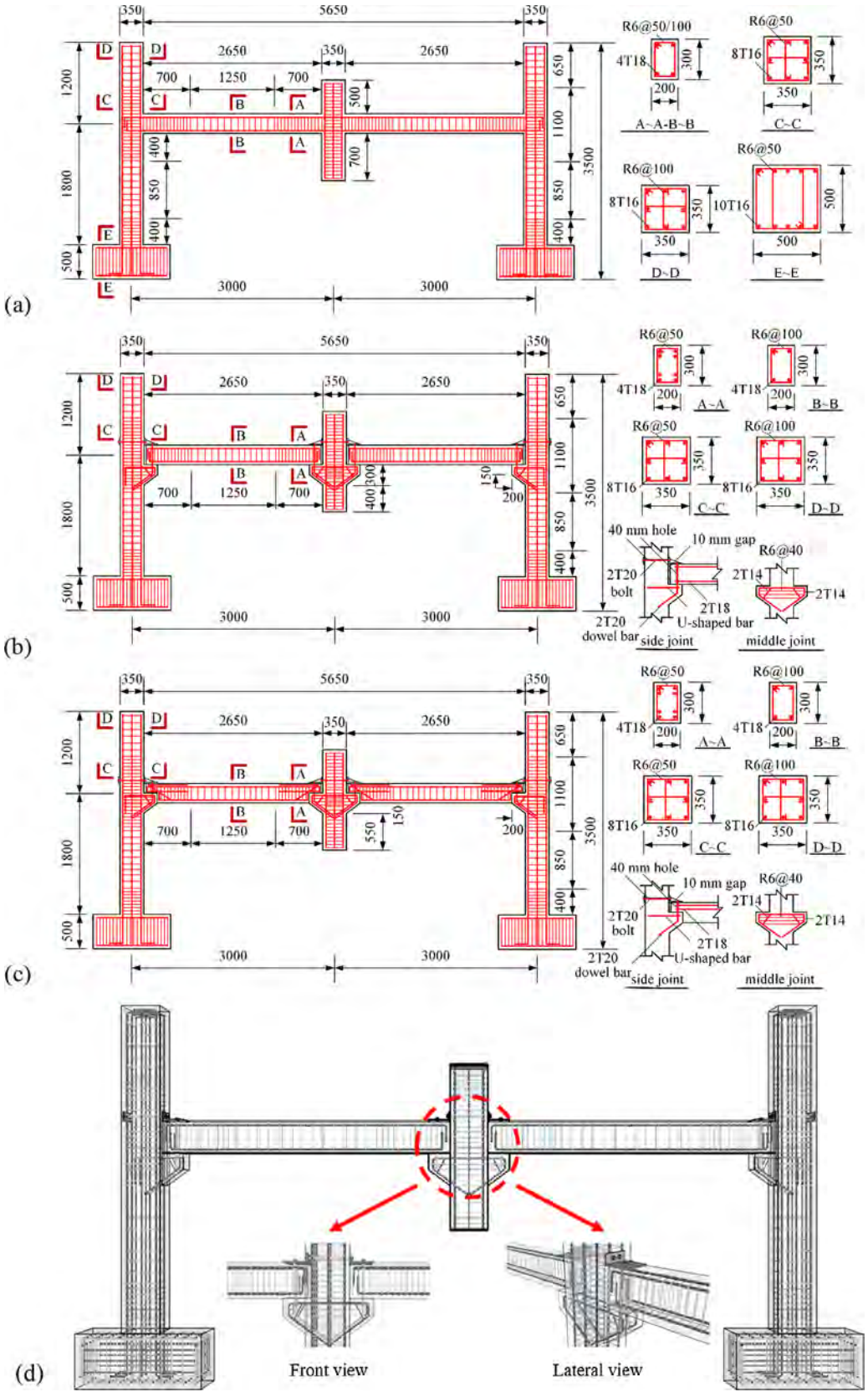

Fig. 1. Dimensions and cross sectional details of test specimens: (a) specimen RC; (b) specimen PC1; (c) specimen PC2; (d) three-dimensional sketch of PC specimens.

Table 1
Specimen details (unit: mm).

Specimens	Dimensions				Longitudinal bars			Transverse bars		
	Column section ($b \times h$) (mm)	Column height (H) (mm)	Beam section ($b \times h$) (mm)	Beam length (L) (mm)	Column	Beam	Corbel	Column	Beam	Joint
RC	350 × 350	3000	200 × 300	2650	8T16	4T18	–	R6@	R6@	–
PC1	350 × 350	3000	200 × 300	2630	8T16	4T18	4 T14	50/100	50/100	R6@40
PC2	350 × 350	3000	200 × 300	2630	8T16	4T18	4 T14			R6@40

Note: T16 indicates the deformed bar with 16 mm diameter, and R6 indicates the plain bar with 6 mm diameter.

Table 2
Material properties.

Materials	Types	Yield strength (MPa)	Tensile strength (MPa)	Elongation (%)
Reinforcing bars	R6 (Transverse bar)	385	460	$\delta_5 = 26$, $\delta_{10} = 21$
	T14 (Corbel bar)	465	616	$\delta_5 = 25$, $\delta_{10} = 22$
	T16 (Column bar)	505	630	$\delta_5 = 28$, $\delta_{10} = 23$
	T18 (Beam bar)	485	622	$\delta_5 = 24$, $\delta_{10} = 21$
	T20 (Dowel bar)	493	629	$\delta_5 = 27$, $\delta_{10} = 19$
Concrete	RC: Cube (150 mm × 150 mm × 150 mm): 27.4 MPa; Cylinder ($D \times L$ = 150 mm×300 mm): 24.7 MPa			
	PC: Cube (150 mm × 150 mm × 150 mm): 37.6 MPa; Cylinder ($D \times L$ = 150 mm×300 mm): 28.3 MPa			
Grouting	PC: Cube (100 mm × 100 mm × 100 mm): 43.4 MPa			

Note: δ_5 and δ_{10} indicate the elongation of the tensile bar with tagging length of 5 and 10 times diameter, respectively.

specimen PC2, the top section (i.e., depth of 150 mm) of the PC beam ends was extruded to cover the corbel. This connection detail may reduce the depth of the exposed corbel.

2.2. Materials

Table 2 shows the material properties. HRB400 deformed bar was used for longitudinal bars of the beam and column, dowel bars, and reinforcement of the corbel. The yield and tensile strengths were 465–505 MPa and 616–630 MPa, respectively. HPB300 plain bar was used for transverse bars of the beam, column, and joint. The yield and tensile strengths were 385 MPa and 460 MPa, respectively. C35 concrete strength of cylinder was 24.7 MPa and 28.3 MPa in cast-in-place concrete and precast concrete, respectively. C50 grouting material of cube was 43.4 MPa.

2.3. Test setup and instrumentation

Fig. 2 shows the setup and instrumentation of the static progressive collapse loading test. The mid-column was constrained by the in-plane constraint frame to resist any possible rotation when fracture of beam rebars occurred at only one side, and steel frames were used to prevent out-of-plane displacement (Fig. 2(b)), so that the only vertical displacement was applied to the mid-column [19]. The top end of exterior

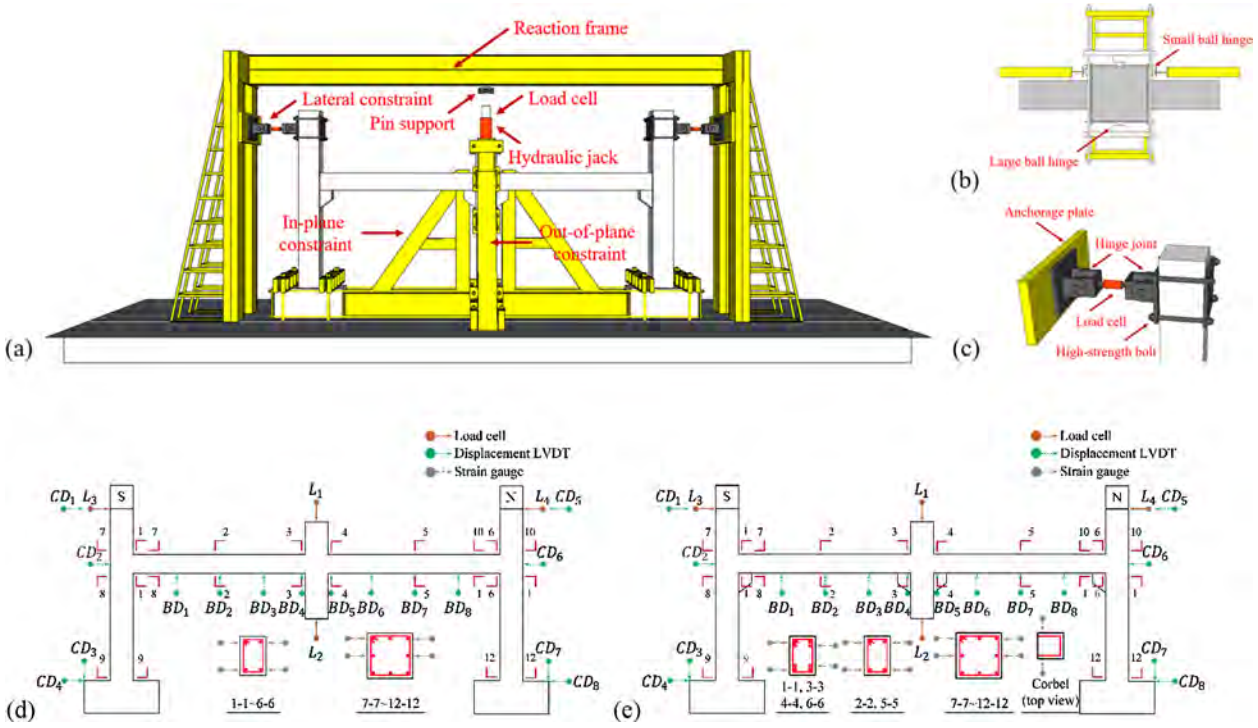

Fig. 2. Test setup and instrumentation: (a) boundary conditions; (b) mid-column constraints; (c) pin support at exterior column; (d) RC specimen; (e) PC specimens.

columns was pin supported, and the horizontal reaction force was measured by a load cell (Fig. 2(c)). Fixed boundary condition was used at the foundation. A hydraulic jack was used to apply the vertical load at the top of the mid-column, and the other one was installed at the bottom of the mid-column for unloading before the test (L_1 and L_2 in Fig. 2(d) and (e)). Lateral reaction force of exterior columns was measured (L_3 and L_4). The vertical displacements of the mid-column and beam were measured by eight linear variable differential transformers (LVDTs) at the location of BD_1 to BD_8. Four LVDTs were used to measure the lateral displacements of the exterior columns (CD_1, CD_2, CD_5, and CD_6), and the displacement of footings was measured by additional four LVDTs (CD_3, CD_4, CD_7, and CD_8). To measure strain distribution of reinforcing bars, 48 strain gauges were attached to the longitudinal bars of the beam and column, and two strain gauges were additionally attached to the dowel bars.

2.4. Loading plan

A hydraulic jack with a load cell was installed on the upper surface of the mid-column to apply axial loading. Before the beams were placed, the bottom hydraulic jack with a load cell was installed to resist the beam self-weight (i.e. simulation of the actual assembling situation). During the test, the bottom hydraulic jack was gradually retracted to release the axial force as the mid-column was being intact, and the dead load due to the self-weight of the specimen and top hydraulic jack was measured from the bottom load cell. A pseudo-static loading was applied using a hydraulic jack on the upper surface of the mid-column until the specimen failed. The force discrepancy between the top and bottom load cells indicates the external vertical load applied to the specimen. The force-controlled loading mechanism was employed at the initial stage of the test (i.e., 3 kN decrease at each step of unloading stage, and 5 kN increase at each step of loading stage). After the peak strength, displacement-controlled loading with the increase of 25 mm at each step was conducted.

3. Test results

3.1. Load-displacement relationship and failure modes

Fig. 3(a) and Table 3 show the vertical load-displacement relationships at the mid-column of the specimens. Fig. 4 shows the specimen damage at the end of the test. In specimen RC, the peak strength in CAA was 119.2 kN when the vertical displacement δ of the mid-column reached 130.9 mm, and the load-carrying capacity in CTA increased to 145.3 kN at δ = 613.9 mm that was 22% greater than that of CAA. At early loading stage in CAA (at δ = 0.8 mm), flexural cracks were initialized in beams, but structural stiffness was not significantly decreased by the effective lateral constraints of exterior columns. The stiffness degradation of the beam was mainly caused by flexural yielding of the beam bottom bars near the mid-column and the beam top bars near the exterior column. When the exterior beam-column joint returned to the original position at δ = 423.5 mm, the load-carrying capacity was increased by tension force of the beam rebars due to the axial constraint of exterior columns under CTA. After the peak strength in CAA, the load resistance was developed relative steadily and significantly increased in CTA. Large cracks and gaps were developed at the beam-column joint interface due to the first bar fracture at δ = 441.7 mm. Further, concrete crushing occurred at the beam bottom near the exterior column and the beam top near the mid-column. Ultimately, fracture of five longitudinal bars of the beam occurred under CTA at δ = 613.9 mm as shown in Fig. 4(a): two beam bottom bars at the left beam near the mid-column (Section C), one beam bottom bar at the right beam near the mid-column (Section D), and two beam top bars in the right exterior beam-column joint (Section B).

In specimen PC1, the peak strength in CAA was 90.9 kN at δ = 100.5 mm, which was 76% of that of specimen RC. Initial flexural cracks were concentrated to the interface of the beam-column joints and beam-corbel joints at δ = 1.6 mm. In the exterior beam-column joint, tension force of the beam top bars was transmitted by the dowel bars, and the beam bottom was supported by the corbel. In the interior beam-column joint, compression force of the beam was resisted by both the dowel bars and mid-column bearing, and tension force of the bottom bars was transmitted by the dowel bars. Because damage and deformation were concentrated to the beam-column joint, the structural behavior of the beam-column joint was closed to hinge behavior, which decreased the load-carrying capacity in CAA. After the peak strength in CAA, the load resistance was decreased rapidly, and CTA was not developed due to the insufficient structural integrity of the beam-column joint. Ultimately, reinforcing bars in corbels were exposed by concrete delamination at δ = 443.4 mm (Fig. 4(b)). Warping occurred in the steel angle cleat at the mid-column due to large rotation of the beam-column joint, and concrete crushing occurred at the exterior beam ends, which caused the geometrically unstable beam. In the exterior beam-column joints, shear fracture of three dowel bars occurred at the interface between the steel angle cleat and PC beam when the vertical displacement δ of the mid-column reached 353.8 mm, 378.5 mm, 406.0 mm, and 443.4 mm, and the load-carrying capacity was significantly decreased. Due to the lack of effective continuous reinforcements in the beam-column joint, the load resistance was significantly affected by the dowel bar strength and concrete compressive strength instead of the beam rebar strength.

In specimen PC2, the peak strengths in CAA and CTA were 96.9 kN (at δ = 96.9 mm) and 76.2 kN (at δ = 474.9 mm), which were 81% and 52% of those of specimen RC, respectively. After the peak strength, CTA

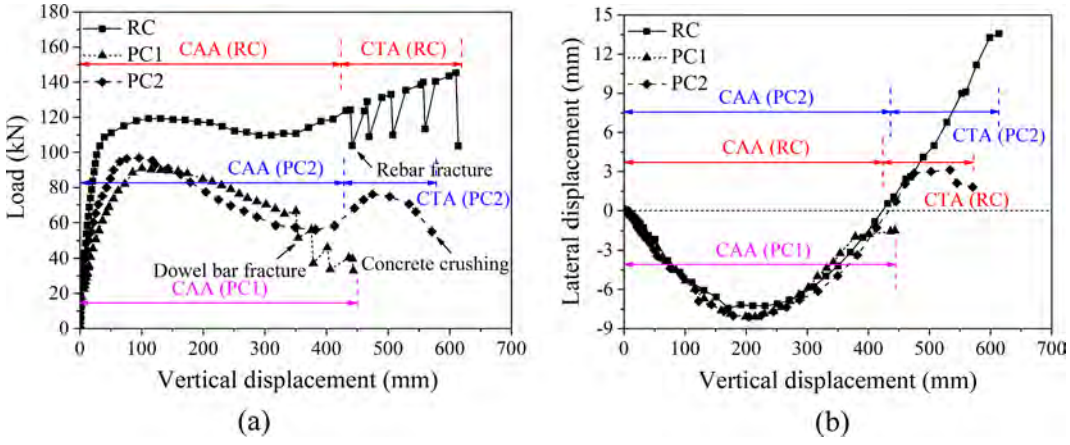

Fig. 3. Test results: (a) load-displacement relationship; (b) lateral displacement of exterior joint.

Table 3
Test results.

Specimens	CAA peak values		Min. (kN)	OP (mm)	CTA peak values		Peak disp. of exterior joint (mm)	Failure modes
	Load (kN)	Disp. (mm)			Load (kN)	Disp. (mm)		
RC	119.2	130.9	109.7	423.5	145.3	613.9	7.44/13.56	Fracture of beam rebar
PC1	90.9	100.5	–	–	–	–	8.11/–	Shear failure of dowel bar
PC2	96.9	95.95	56.1	434.1	76.2	474.9	8.09/3.12	Concrete crushing

Note: Min. indicates the minimum load after the 1st peak strength; and OP indicates the mid-column displacement corresponding to the exterior joint displacement of zero.

was temporarily developed, and the beam top bars near the mid-column were yielded in compression. The damage pattern of specimen PC2 was similar with that of specimen PC1. However, concrete crushing occurred in the corbel and beam ends at $\delta = 570.9$ mm, and large gaps occurred at the interface between the beam bottom and corbel of the mid-column (Fig. 4(c)). As a result, the load transmission mechanism was developed by the extruded beam region. Ultimately, concrete crushing of the beam end and corbel caused the geometrically unstable system.

Fig. 3(b) shows the relationships between the lateral displacement of the exterior joint (i.e., average value of CD_2 and CD_6 in Fig. 2) and the vertical displacement of the mid-column. The positive and negative values indicate the inward and outward movements of the exterior joint, respectively. In all specimens, the outward displacement of the exterior joint occurred at initial stage, which reached the maximum value at the mid-column displacement of 200 mm corresponding to two-thirds of the beam height. In specimen RC, the outward displacement of the exterior joint decreased to zero after the peak outward displacement of 7.44 mm. As the vertical displacement of the mid-

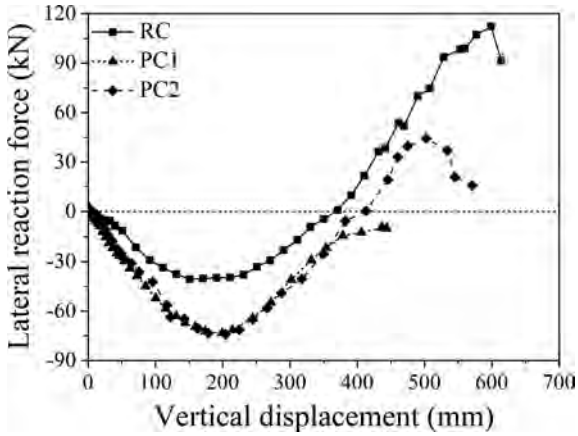

Fig. 5. Lateral reaction force.

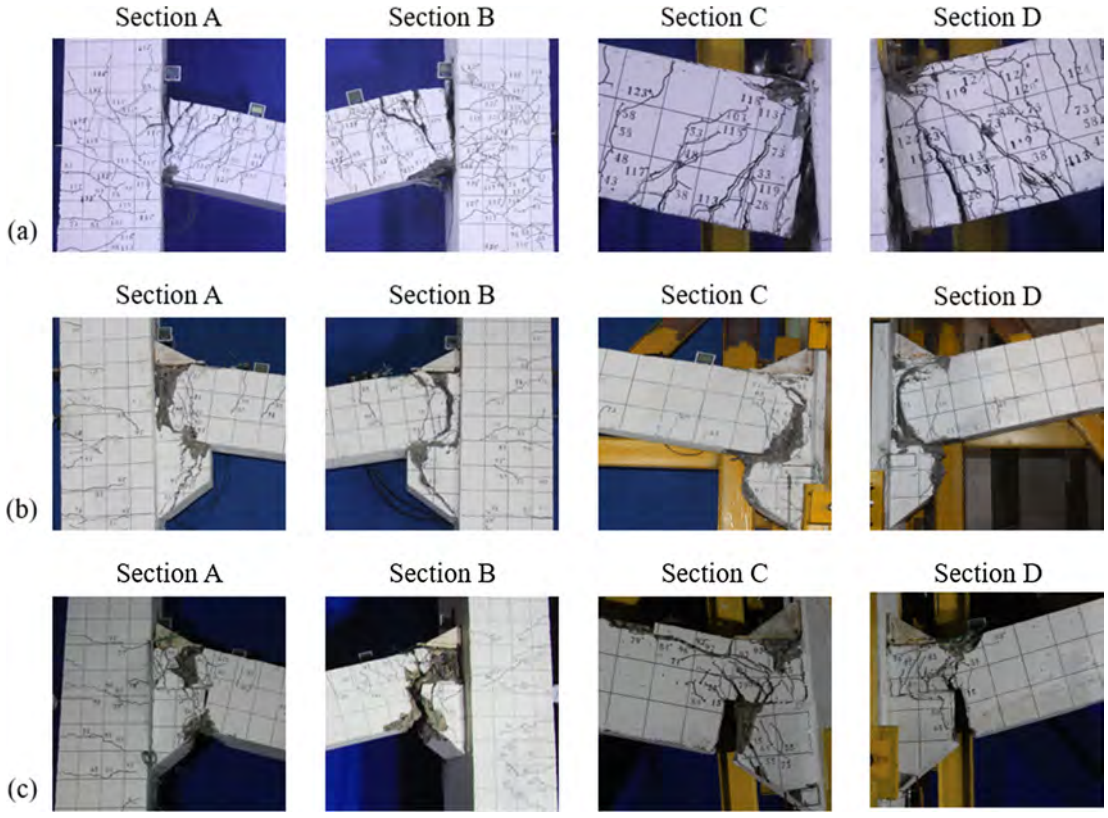

Fig. 4. Damage patterns of specimens: (a) specimen RC; (b) specimen PC1; (c) specimen PC2 (Section A denotes the left exterior joint, Section B denotes the right exterior joint, Section C denotes the left side of interior joint, and Section D denotes the right side of interior joint).

Table 4
Constraint stiffness of exterior columns.

Specimens	Peak outward values		Peak inward values		Characteristic values		Constraint stiffness (kN/mm)		
	Load (kN)	Disp. (mm)	Load (kN)	Disp. (mm)	Load (kN)	Disp. (mm)	Left	Right	Average
RC	40.8	5.777	112.27	11.091	117.73	391.1	8.99	9.12	9.06
PC1	73.4	6.577	–	–	–	–	10.87	12.06	11.47
PC2	74.2	6.962	44.37	3.512	63.2	438.25	10.71	11.51	11.11

Note: Characteristic values indicate the load and displacement of the mid-column when the compression/tension force or the outward/inward displacements of exterior columns changed.

column increased, the inward displacement of the exterior joint increased to 13.56 mm due to the large contribution of CTA. In specimens PC1 and PC2, the peak outward displacement reached 8.11 mm and 8.09 mm, respectively. However, specimen PC1 failed at the outward displacement of 1.49 mm (i.e., without CTA). Specimen PC2 generated only the inward displacement of 3.12 mm, which indicates the contribution of CTA to the progressive collapse resistance of the fully assembled PC specimens is not significant.

3.2. Constraint stiffness of exterior columns

Fig. 5 compares the average lateral reaction force at the inflection point of two exterior columns in the three specimens. Similar to the lateral displacement of the exterior columns, compression force was developed in CAA of all specimens, but tension force was developed in CTA of specimens RC and PC2. The maximum compressive force of specimen RC reached 40.8 kN, which was less than that of specimens PC1 (73.4 kN) and PC2 (74.2 kN). This is because rotation of the beam ends at the beam-column joint interface in PC specimens with semi-rigid connection increases the compression force in CAA stage. The maximum lateral tension force of specimen RC (112.7 kN) was greater than that of specimen PC2 (44.3 kN).

Because the steel reaction frame does not have infinite stiffness, the relationship between the lateral reaction force and corresponding displacement should be estimated for numerical analysis (refer to the chapter of "**Finite Element Analysis**"). Table 4 shows the constraint properties of the exterior column determined from the Levenberg-Marquardt method where the relationship between the lateral reaction and displacement can be linearly defined [36]. The constraint stiffness of specimen RC was identified as 8.99 kN/mm in the left side and 9.12 kN/mm in the right side, which showed the almost symmetric constraint. In the PC specimens, the average constraint stiffness of 11.47 kN/mm for specimen PC1 and 11.11 kN/mm for specimen PC2 was greater than that of specimen RC.

3.3. Deformation of beams and columns

Fig. 6 shows the global deformation of test specimens. In specimen RC, when the vertical displacement of the mid-column was 211 mm, the maximum outward displacements of the left exterior column were 6.59 mm at the joint and 5.55 mm at the column top, and the maximum outward displacements of the right exterior column were 7.91 mm at the joint and 5.95 mm at the column top (Fig. 6(a) and (c)). Under CTA, the maximum inward displacements of the left exterior column were 15.74 mm at the joint and 14.02 mm at the column top, and the maximum inward displacements of the right exterior column were 11.88 mm at the joint and 9.19 mm at the column top. As shown in Fig. 6(b), symmetric deflection occurred in the beam until the vertical displacement of the mid-column reached 614 mm, and the mid-column was tilted due to bar fracture of the right beam. In specimen PC1, shear failure of dowel bars in the interior joint caused asymmetric deflection of the beam when the vertical displacement of the mid-column reached 443 mm (Fig. 6(e)). The outward displacement of specimen PC1 was similar to that of specimen RC (Fig. 6(d) and (f)), in which the maximum outward displacements of the exterior joint and column top were 8.99 mm and 6.58 mm in the left column, and 7.23 mm and 6.57 mm in the right column, respectively. In specimen PC2, the mid-column was tilted when the vertical displacement reached 571 mm due to concrete crushing at the beam end (Fig. 6(h)). The outward displacement of specimen PC2 was greater than that of specimen RC, while the inward displacement of specimen PC2 was less than that of specimen RC (Fig. 6(g) and (i)). Under CAA, the maximum outward displacements of the exterior joint and column top were 8.59 mm and 6.94 mm in the left column, and 7.60 mm and 4.66 mm in the right column, respectively. Under CTA, the maximum inward displacement of the exterior joint was less than that of the column top because of temporary development of CTA.

3.4. Rebar strain

Fig. 7 shows the strain distribution of longitudinal bars of beams. In specimen RC, as the vertical displacement of the mid-column increased, compressive strain of the top bar increased in the beam near the mid-column, while tensile strain of the top bar increased in the beam region under negative moment (Fig. 7(a)). After rebar yielding, tensile strain of the top bar at the beam ends was significantly increased and then fractured due to CTA. When the applied load reached the minimum value after the 1st peak strength, the maximum compressive strain occurred in the top bar of the beam near the mid-column. After the peak strength, compressive strain of the bottom bar decreased, and then it was transformed into tensile strain (Fig. 7(b)). In specimen PC1, the top bar strain of the beam ends near the mid-column were less than that of specimen RC (Fig. 7(c)). Further, the bottom bar of the beam end near the exterior columns showed tensile strain before the 1st peak strength (Fig. 7(d)). The top bar strain distribution of the beam in specimen PC2 was similar to that of specimen PC1 (Fig. 7(e)). The bottom bar strain of the beam in specimen PC2 was not measured due to the malfunction of the strain gauges. In general, the values of rebar strain in specimens PC1 and PC2 were less than those of specimen RC. This is because the contribution of CTA to the load resistance was not significant in specimens PC1 and PC2.

Fig. 8 shows the strain distribution of longitudinal bars of a right exterior column. As the vertical displacement of the mid-column increased, tensile/compressive strains of the column rebars were converted in specimens RC and PC2. On the other hand, the rebar strain conversion was not occurred in specimen PC1 showing only outward lateral displacement. The outside bars at the exterior joint of the three specimens were tensile yielded in CAA.

4. Finite element analysis

4.1. Element types

To understand the load transfer mechanism of the three specimens subjected to the mid-column removal scenario, finite element analysis was performed using *ABAQUS/Explicit* program. Fig. 9 shows the analysis model of specimen PC1. An eight-node solid element with reduced integration (C3D8R) was employed for concrete modelling of beams,

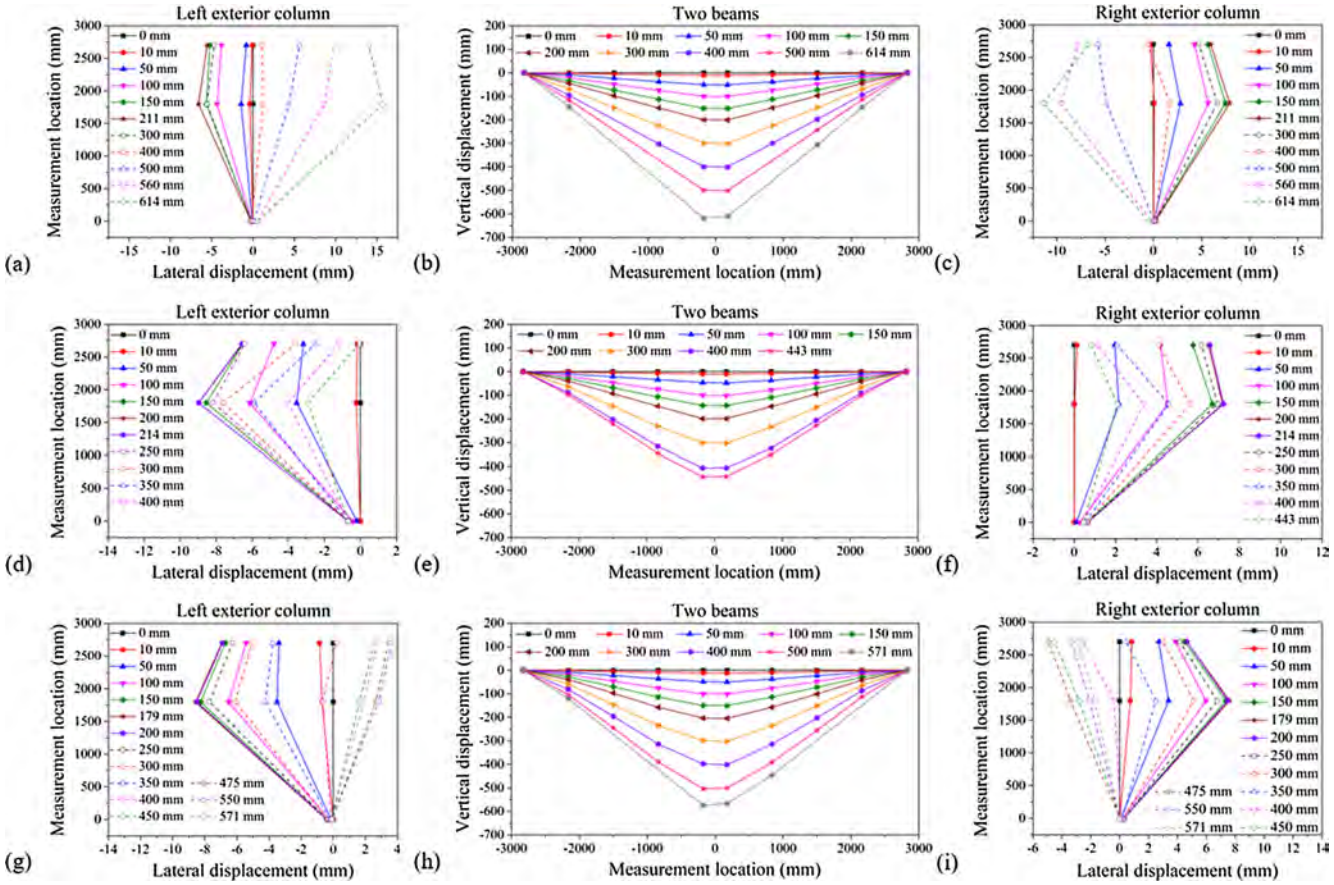

Fig. 6. Global deformation of specimens: (a) left column of specimen RC; (b) beams of specimen RC; (c) right column of specimen RC; (d) left column of specimen PC1; (e) beams of specimen PC1; (f) right column of specimen PC1; (g) left column of specimen PC2; (h) beams of specimen PC2; (i) right column of specimen PC2.

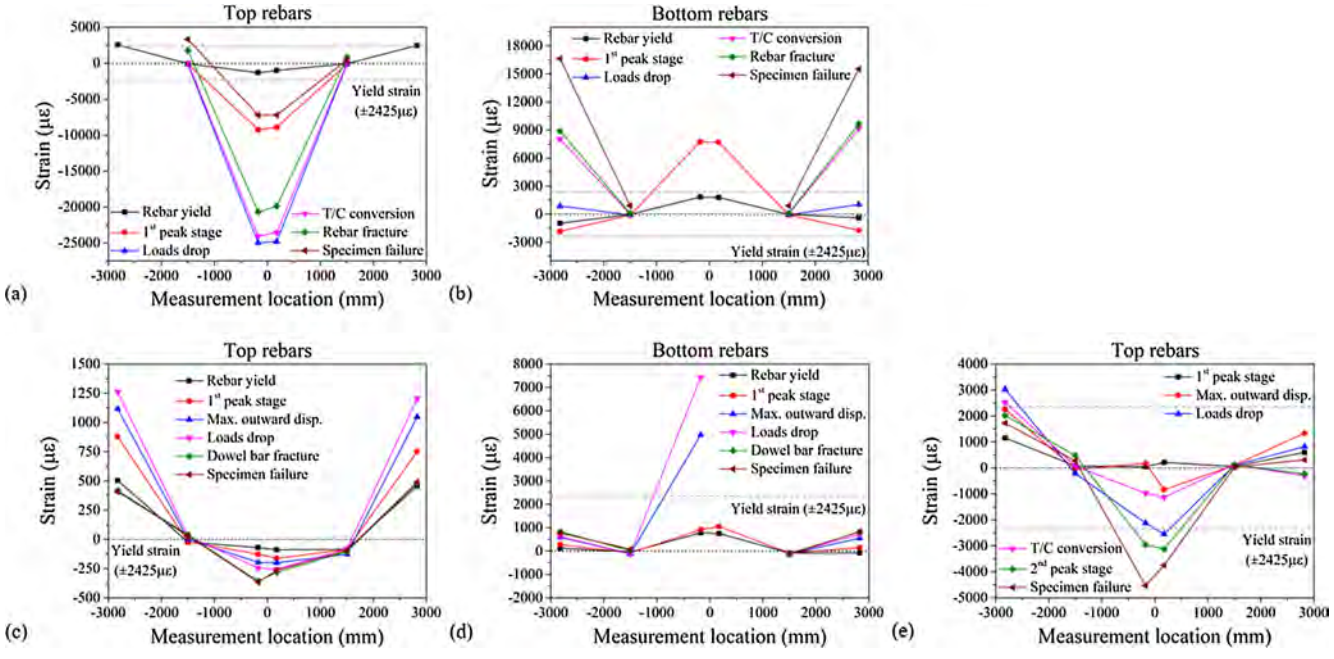

Fig. 7. Strain of beam longitudinal bars: (a) top bars of specimen RC; (b) bottom bars of specimen RC; (c) top bars of specimen PC1; (d) bottom bars of specimen PC1; (e) top bars of specimen PC2.

columns and corbels, and a two-node truss element (T3D2) was employed to simulate reinforcing bars. Dowel bars and steel angle cleats were modelled by the solid element to estimate the stress distribution accurately. Considering the stress distribution of specimens, the mesh size of 20 mm was adopted for the concrete of beam-column joints, while the mesh size of 20 mm was used in both the mid-span of beams and the middle part of columns to improve the calculation efficiency. In steel reinforcements, the mesh size of 50 mm was used. The embedded

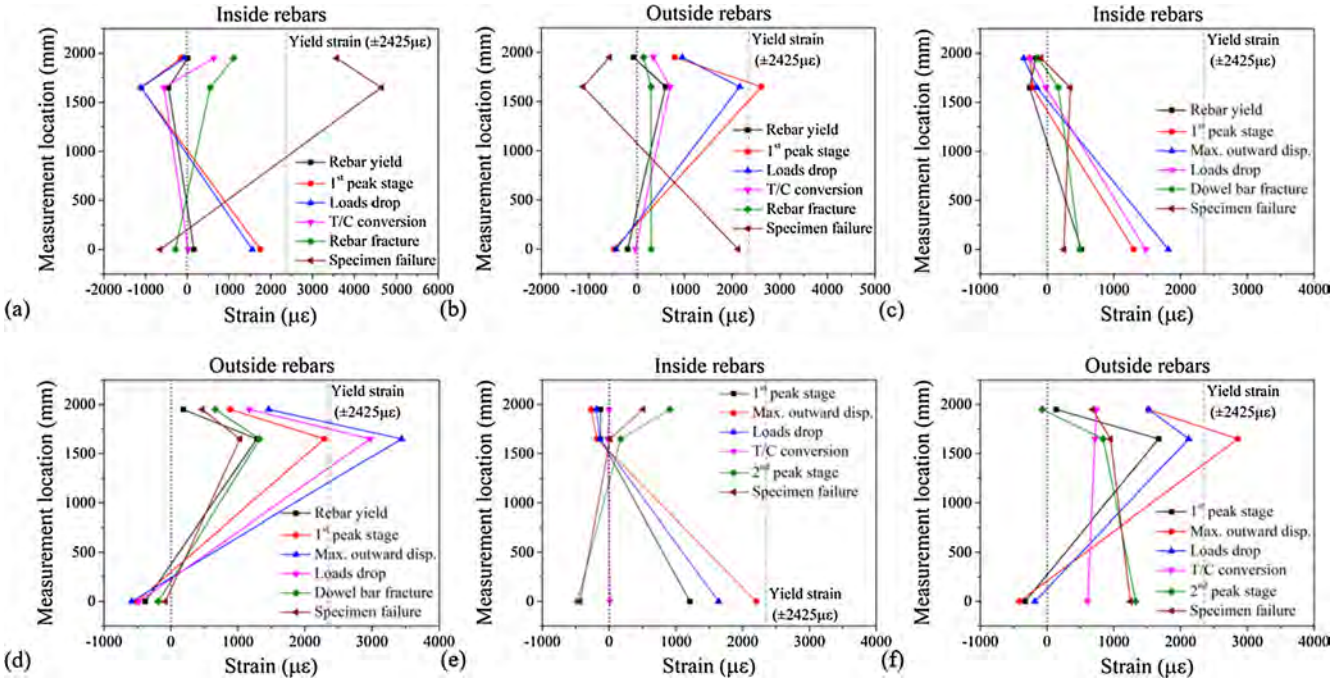

Fig. 8. Strain of right column longitudinal bars: (a) inside bars of specimen RC; (b) outside bars of specimen RC; (c) inside bars of specimen PC1; (d) outside bars of specimen PC1; (e) inside bars of specimen PC2; (f) outside bars of specimen PC2.

constraint was adopted to simulate the bond strength between the steel reinforcements and concrete [37].

4.2. Boundary conditions

Fixed boundary condition was used in the foundation to restrict the displacement and rotation. Spring constraint was employed at the pin support in the top of exterior columns, in which the stiffness values were 9.1 kN/mm for specimen RC, 11.5 kN/mm for specimen PC1, and 11.1 kN/mm for specimen PC2 specimen, on the basis of the test results (refer to Table 4). Tie constraint condition was considered in the interaction surface of the dowel bars and high-strength bolts with the steel angle cleats because the slip was not observed in the test. Friction behavior between different parts in contact was modeled using an isotropic penalty friction formulation, and a friction coefficient of 0.40 was applied to define the friction behavior in the tangential direction. Further, hard contact was utilized to define the pressure behavior of the contact interaction in the normal direction [38].

4.3. Material models

The uniaxial stress-strain relationship of concrete prescribed in GB50010-2010 [32] was employed to simulate the constitutive relationship of concrete component (Fig. 10(a)). Concrete compressive strength measured in the test, elastic modulus of 3×10^4 N/mm^2, Poisson's ratio of 0.2, and density of 2.4×10^3 kg/m^3 were used. Concrete damage plasticity (CDP) model was adapted to consider the nonlinearity, stiffness degradation, and strain rate effect on the material property, which was coupled with fracture energy to ensure the mesh-size independent result [38]. In the CDP model, tensile cracking and compressive crushing of concrete are considered the main two failure mechanisms. On the basis of the smeared cracking approach, the damage or stiffness degradation is assumed to be uniformly distributed. The cracked concrete is regarded as an elastic orthotropic material with a reduced elastic modulus. According to Kwak and Gang [39], the smeared crack concept is suitable for the finite element analysis because the continuity of the displacement field remains intact. In the CDP model, the stiffness degradation is assumed to occur in the softening response in both compression and tension. As shown in Fig. 11, the CDP model modifies the yield surface in the deviatoric plane to consider different yield stresses in tension and compression by using a shape parameter (K_c). Dilation angle (Ψ) is used for plastic flow behavior, and a constant value is assumed during plastic yielding. Plastic potential eccentricity (ϵ) increases the dilation angle. The ratio of the biaxial stress to uniaxial stress (σ_{b0}/σ_{c0}) is considered to describe the material state under multiaxial stress state. In this study, the corresponding parameters were defined as $K_c = 0.6667$, $\Psi = 30$, $\epsilon = 0.1$, and $\sigma_{b0}/\sigma_{c0} = 1.16$ according to the study of Genikomsou and Polak [40].

To describe the stress-strain relationship of longitudinal bars, the trilinear isotropic hardening model was employed addressing

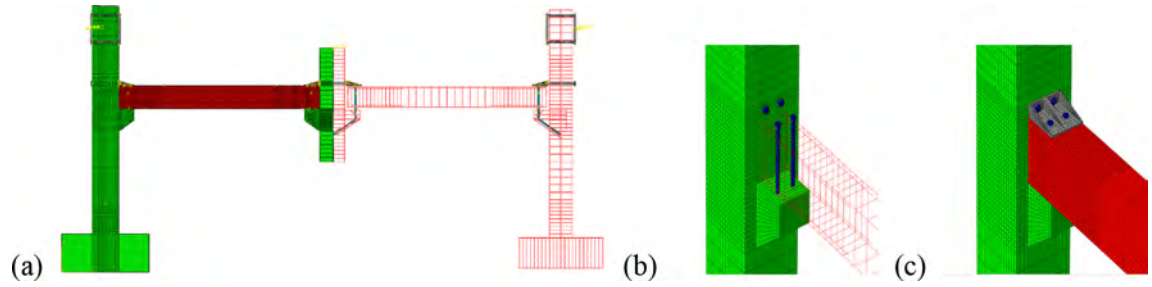

Fig. 9. Analysis model of specimen PC: (a) model details; (b) details of steel reinforcements; (c) mesh details in beam-column joint.

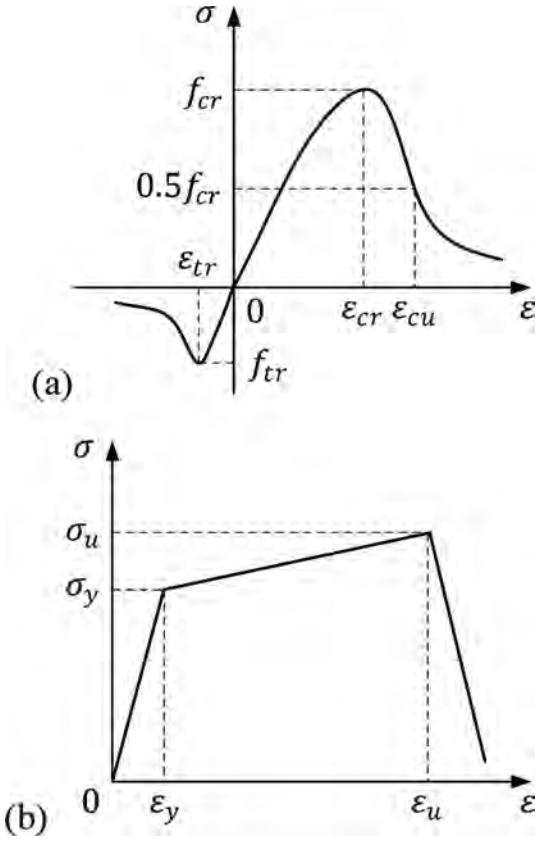

Fig. 10. Stress-strain relationship of materials: (a) concrete; (b) steel reinforcement.

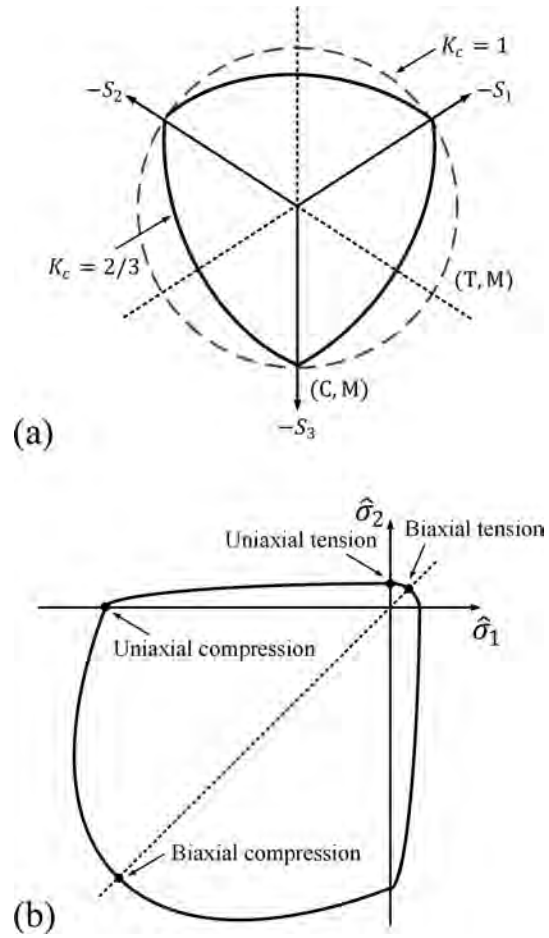

Fig. 11. Illustration of concrete damage plasticity model: (a) deviatoric plane; (b) plane stress yield surface.

the strengthening stage after yielding and the descending stage after fracture (Fig. 10(b)). The ideal elasto-plastic model was used for transverse bars. The constitutive relationship of both the high-strength bolts and steel angle cleats were presented by the bilinear isotropic hardening model. Yield and tensile strength measured in the test, elastic modulus of 2×10^5 N/mm^2, Poisson's ratio of 0.3, and density of 7.8×10^3 kg/m^3 were used.

4.4. Analysis results

Figs. 12–13 and Table 5 compare the test results with the predictions including the load-displacement relationship, lateral displacement of the exterior joint, and local crack distribution. The analysis model predicted well the test results. The average deviation of the load-carrying capacity and ultimate displacement in the three specimens was less than 5%. In specimen RC, a large amount of cracks occurred in the beam end of both the analysis model and specimen (Fig. 13(a)).

In specimen PC1, the peak strength, displacement corresponding to the peak strength, and fracture location of rebars were predicted in a reasonable precision (Fig. 12(b)). However, the prediction showed the rapid strength increment and smooth strength degradation, which was mainly attributed to the neglected grouting detail in the analysis model. The prediction of the lateral displacement of the exterior beam-column joint showed similar tendency with the strength prediction (Fig. 12(e)). Similar to the test results, a large amount of cracks occurred in the outside of the exterior beam-column joint, beam end, and corbel. Tensile strength of the grouting material at the joint interface was ignored, so that gap was formed in the interior beam-column joint. Shear fracture occurred in dowel bars projected from exterior columns, showing large stress level at the connection with a steel angle cleat. On the other hand, the stress state of high-strength bolts was less than yield strength.

In specimen PC2, the prediction in CAA agreed well with the test result (Fig. 12(c) and (f)). Both the analysis and test results showed the strength degradation in CTA due to fracture of dowel bars before the 2nd peak strength. The analysis model predicted local damage of concrete at the connection between the beam and corbel, but the 2nd peak strength prediction was earlier and greater than that of the test result. Dowel bars embedded in the corbel of the exterior column were partly deformed, and the largest stress was evaluated at the interface with the steel angle cleat. The dowel bar failure decreased the load-carrying capacity significantly during the development stage of CTA. The stress state of high-strength bolts in specimen PC2 was relatively greater than that of specimen PC1.

5. Parametric study

5.1. Effect of dowel bar

According to the test results of the PC specimens, critical failure occurred at the beam end connection: dowel bar failure in specimen PC1; and concrete crushing of the beam end in specimen PC2. To improve the structural reliability, a parametric study was performed considering the dowel bar as a design parameter. In specimens PC1-1 and PC2-1, two kinds of high-strength bolts were used for the dowel bar (i.e. yield strength of 800 MPa and 1000 MPa). In specimens PC1-2 and PC2-2, dowel bar diameter was increased from 20 mm to 25 mm.

Fig. 14 shows the variations of the analysis results according to the dowel bar. The results showed that new dowel bars increased the 2nd peak strength significantly, which was greater than the 1st peak strength (Fig. 14(a) and (b)). As shown in Fig. 14(c) and (d), the inward

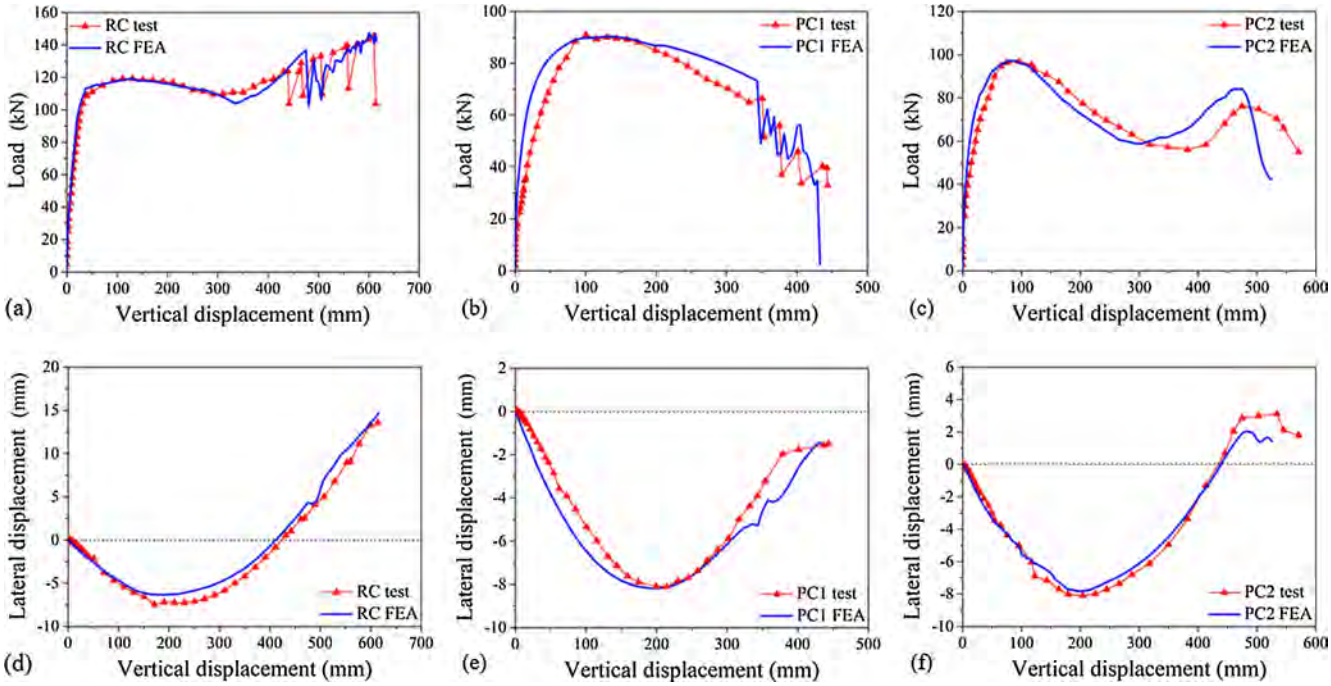

Fig. 12. Comparison between test and FEA results: (a) mid-column displacement of specimen RC; (b) mid-column displacement of specimen PC1; (c) mid-column displacement of specimen PC2; (d) lateral displacement of specimen RC; (e) lateral displacement of specimen PC1; (f) lateral displacement of specimen PC2.

displacement of the exterior joint increased, which improved the contribution of CTA to the progressive collapse performance. The load-carrying capacity of specimens PC1-1 and PC1-2 at CAA was 31% and 13% greater than that of specimen PC1, respectively. As a result, the 1st peak strength of specimen PC1-1 and PC1-2 reached 100% and 86% of that of specimen RC. Further, the 2nd peak strength of specimen PC1-1 and PC1-2 increased to 98% and 77% of that of specimen RC. Ultimately, specimens PC1-1 and PC1-2 failed due to fracture of beam rebars and dowel bar failure, respectively. The load-carrying capacity of specimens PC2-1 and PC2-2 at CAA was the same to that of specimen PC2, while the 2nd peak strength at CTA was increased by 161% and 120%, respectively. Compared to specimen RC, the 1st peak strength of specimens PC2-1 and PC2-2 was just 80% and 81% of that of specimen RC, but the 2nd strength was 37% and 15% greater than that of specimen RC. Ultimately, specimens PC2-1 and PC2-2 failed due to fracture of beam rebars.

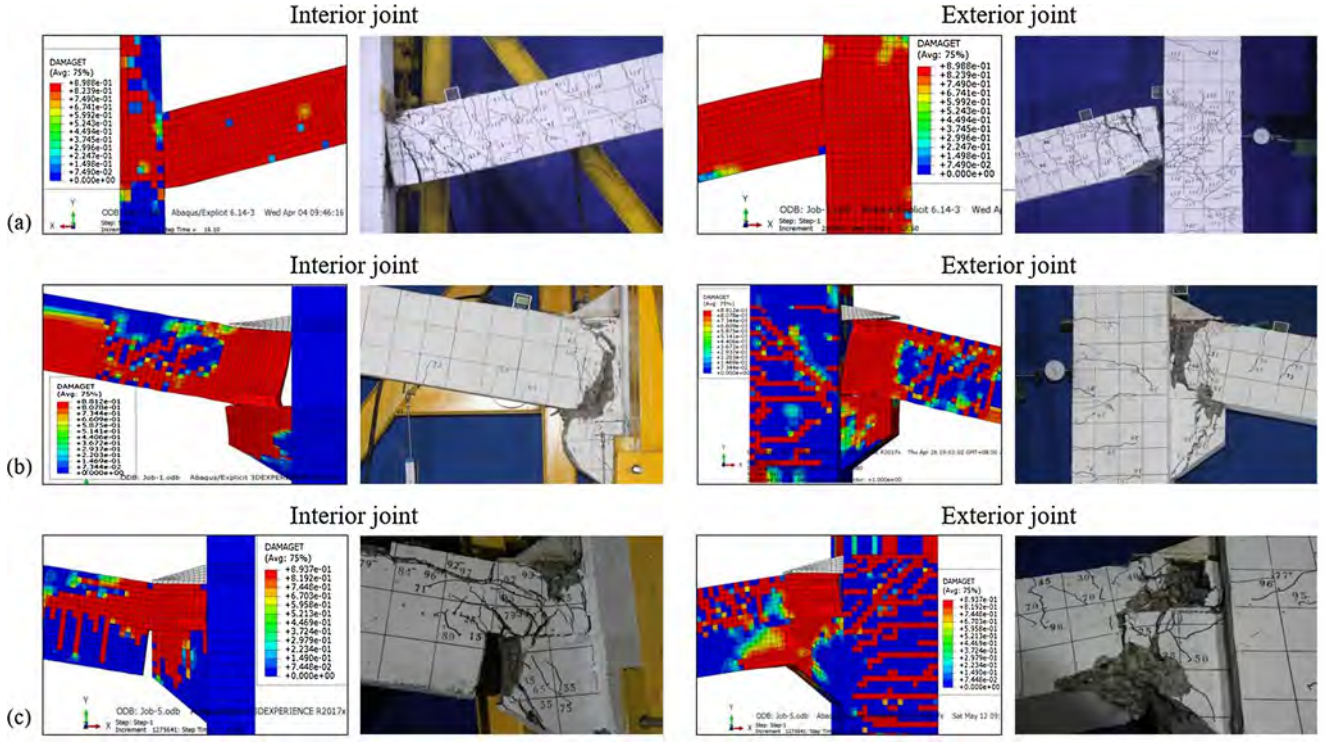

Fig. 13. Comparison of damage patterns between test and FEA results: (a) specimen RC; (b) specimen PC1; (c) specimen PC2.

Table 5
Analysis results.

Specimens		1st peak values		OP (mm)	2nd peak values		Peak disp. of exterior joint (mm)	Failure modes
		Load (kN)	Disp. (mm)		Load (kN)	Disp. (mm)		
RC	Test	119.2	130.9	423.5	145.3	613.9	7.4/13.6	Fracture of beam rebar
	Analysis	119.5	128.2	413.9	147.1	613.1	6.3/14.5	Fracture of beam rebar
PC1	Test	90.9	100.5	–	–	–	8.1/–	Shear failure of dowel bar
	Analysis	89.8	98.8	–	–	–	8.2/–	Shear failure of dowel bar
PC2	Test	96.9	95.95	434.1	76.2	474.9	8.1/3.1	Concrete crushing
	Analysis	97.3	92.6	438.5	84.3	464.4	7.8/1.7	Shear failure of dowel bar

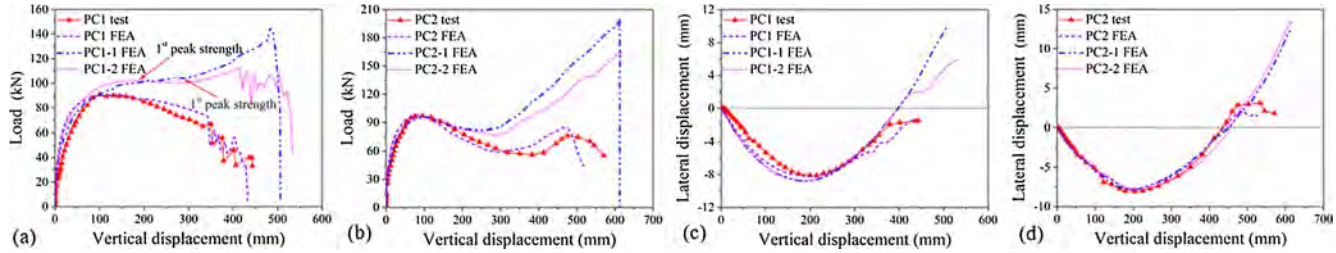

Fig. 14. Analysis results according to dowel bar design: (a) load-displacement relationship of specimen PC1; (b) load-displacement relationship of specimen PC2; (c) lateral displacement of specimen PC1; (d) lateral displacement of specimen PC2.

Table 6
Types of steel angle cleats (unit: mm).

Specimens	Analysis cases	Length of Side-1	Length of Side-2	Thickness
PC1-3	No steel angle cleats	–	–	–
PC1-4	Without side plate	60	200	10
PC1-5	With one side plate	60	200	10
PC1-6	With two side plates	60	200	10
PC1-7	Without side plate	200	200	10
PC1-8	With one side plate	200	200	10

Note: Side-1 and Side-2 indicate the length of angle cleat limbs which is perpendicular and parallel to the beam, respectively.

5.2. Effect of steel angle cleat

In specimens PC1 and PC2, the steel angle cleat stiffened with three side plates was installed on the top face of the beam end for better load transmission to the beam-column joint. To investigate the effect of steel angle cleat configuration on the load-carrying capacity, a parametric study was performed in specimen PC1. Table 6 shows the six details of the steel angle cleat. Fig. 15 shows the stress distribution of the steel angle cleat. When the side plates are removed, stress concentration occurred at bolt holes (Fig. 15(b)). For the steel angle cleat strengthened by one side plate, large stress was developed at the center of the side plate (Fig. 15(c)), and the stress distribution was similar to that of the steel angle cleat with two and three side plates (Fig. 15(a) and (d)). When the dimensions of the steel angle cleat increased, large deformation occurred around the bolt holes (Fig. 15(e) and (f)).

Fig. 16(a) shows the load-displacement relationship of specimens with various configurations of steel angle cleats. Specimen PC1-3 without the steel angle cleat exhibited the least load resistance (i.e., 58.9% and 59.7% of the peak strength of test and analysis results in specimen PC1, respectively), which indicates that the steel angle cleat affects the structural resistance mechanism significantly. The peak strength of specimen PC1-4 was 91.9% and 93.0% of that of test and analysis results in specimen PC1. Compared to the steel angle cleat without side plates, the addition of one and two side plates (specimens PC1-5 and PC1-6) increased the peak strength by 6.9% and 8.2%, respectively (99.5% and 100.7% of the peak strength prediction in specimen PC1). The peak strength of specimen PC1-5 was slightly less than that of specimen PC1-6, but the load-displacement relationships of the

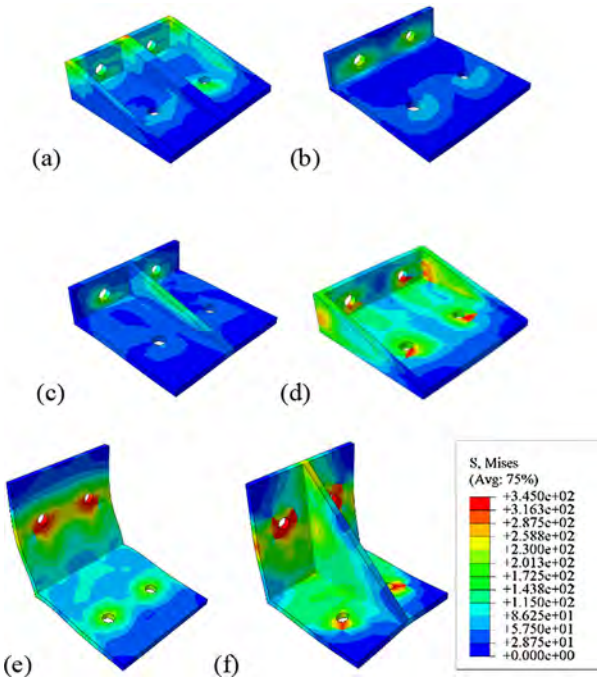

Fig. 15. Stress distribution of steel angle cleat: (a) PC1; (b) PC1-4; (c) PC1-5; (d) PC1-6; (e) PC1-7; (f) PC1-8.

both specimens agreed well with that of specimen PC1. This result indicates that the steel angle cleat with multi-legs (with two side plates) or triple-legs (with three side plates) is not effective to increase the peak strength. Due to large deformation of the steel angle cleat in specimen PC1-7, the peak strength and deformation capacity of specimen PC1-7 were less than those of specimen PC1-4. Similarly, specimen PC1-5 exhibited better load-carrying capacity than PC1-8 under large displacement. The analysis results showed that the load-carrying capacity would be enhanced by the steel angle cleat, but the strengthening effect was limited at the steel angle cleat with multi-legs. Further, the steel angle cleat with unequal-leg exhibited better performance than that of equal-leg when the same number bolts were used.

Fig. 16(b) shows the lateral displacement of the exterior joint of

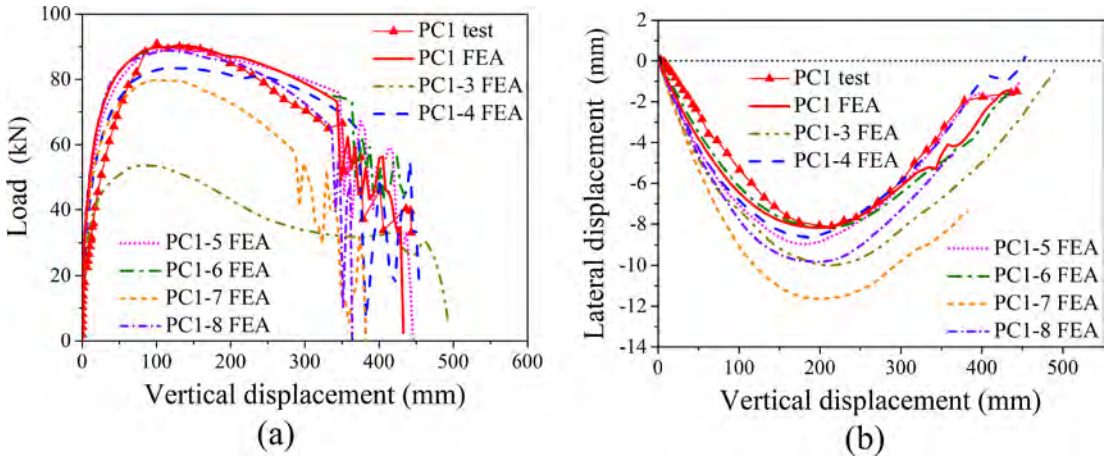

Fig. 16. Analysis results according to steel angle cleat: (a) load-displacement relationship; (b) lateral displacement of exterior joint.

specimens with various steel angle cleats. The largest outward displacement occurred in specimen PC1-7, and the least displacement was occurred in specimen PC1. The analysis result showed that larger stiffness of the steel angle cleat decreased the outward displacement of the exterior joint, while the effect was not significant among the steel angle cleats with multi-legs. In specimens PC1-3, PC1-7 and PC1-8 showing the large lateral displacement, shear failure of dowel bars occurred at the joint interface between the mid-corbel and beam. On the other hand, in other specimens, shear failure of dowel bars projected from the exterior corbel occurred at the interface between the top of beam end and steel angle cleat.

6. Conclusions

In the present study, static loading test was performed in one half scale RC and two half scale PC moment sub-structures to investigate the progressive collapse performance. For fully assembled PC joint, two connection details using the dowel bar, corbel, and steel angle cleat were applied to specimens PC1 and PC2. The structural performance including the load-carrying capacity, deflection, lateral displacement, rebar strains, crack distribution and failure modes were evaluated. The principal conclusions are summarized as follows:

(1) Specimens under the removal of the mid-column scenario showed two load resistance mechanism. In specimen RC, compression force of CAA increased the beam moment strength due to P-M interaction. After the 1st peak strength, large deformation of the specimen changed the beam bar stress from compression to tension, which caused the 2nd peak strength in CTA that improves the progressive collapse performance. On the other hand, in specimen PC1 with the PC beam sitting on the corbel, the load-carrying capacity was significantly decreased after the 1st peak strength because of dowel bar fracture. Although CTA was developed in specimen PC2 with the extruded PC beam covering the corbel, the 2nd peak strength was less than the 1st peak strength due to concrete crushing of beam ends.
(2) The peak strength of specimen RC in CTA was 22% greater than that in CAA. Ultimately, specimen RC failed due to fracture of beam longitudinal bars at the plastic hinge. Unlike specimen RC, the majority of the damage of specimens PC1 and PC2 occurred in the beam-column connection. As a result, the load-carrying capacity of specimens PC1 and PC2 was less than that of specimen RC. The weak connection integrity decreased the load-carrying capacity of specimens PC1 and PC2 to 76% and 81% of that of specimen RC specimen in CAA, respectively. Further, the ultimate displacement of the mid-column in specimens PC1 and PC2 was 72% and 77% of that of specimen RC.
(3) Finite element analysis was conducted in *ABAQUS* program to discuss the failure behavior of test specimens. The analysis results agreed well with the test results including the load-displacement relationship, crack pattern, and failure mode. Large stress occurred in the dowel bar at the connection with the steel angle cleat, which caused shear failure of the dowel bar.
(4) To evaluate the effects of dowel bar and steel angle cleat on the structural performance, a parametric study was performed. The use of large diameter or high-strength in the dowel bar improved the contribution of CTA to the structural performance of PC specimens. Further, for optimal design of PC beam-column connections, the use of the steel angle cleat is recommended in practical application.

Declaration of Competing Interest

The authors declare that they have no competing financial interests for this paper.

Acknowledgements

The authors sincerely appreciate the funding support provided by the National Key Research and Development Program of China (No. 2016YFC0701400, 2016YFC0701308), the Key Research and Development Program of Hunan Province (No. 2017SK2220), the National Natural Science Foundation of China (NSFC) (No. 51878264), the Research and Develpment Program of Changsha City (No. kq1706019), and the Ministry of Land, Infrastructure, and Transport Affairs of the Korean Government (Grant No. 14-RERP-B082884-01 from the Housing Environmental Research Project).

References

[1] Ellingwood BR. Mitigating risk from abnormal loads and progressive collapse. ASCE J Perform Constr Facil 2006;20(4):315–23.
[2] Hong JK, Kang TH-K. Computing in Protection Engineering: CFD Analysis of Blade Fragment Impact on Concrete Wall. J Struct Integrity Maint 2018;3(4):210–6.
[3] Lee M, Kwak H-G. Blast and Impact Analyses of RC Beams Considering Bond-Slip Effect and Loading History of Constituent Materials. Int J Concr Struct M 2018;12(32).
[4] Ellingwood BR, Leyendecker EV. Approach for design against progressive collapse. J Struct Divis 1978;104:413–23.
[5] Lu XZ, Zhang L, Lin KQ, Li Y. Improvement to composite frame systems for seismic and progressive collapse resistance. Eng Struct 2019;186:227–42.
[6] Ersoy U, Tankut T. Precast concrete members with welded plate connections under reversed cyclic loading. PCI J 1993;38(4):94–100.
[7] PCI (Precast Prestressed Concrete Institute). PCI design handbook. 7th ed.; 2010.
[8] Vidjeapriya R, Jaya KP. Behaviour of precast beam-column mechanical connections under cyclic loading. ASCE J Perform Constr Facil 2012;13(2):233–45.
[9] GSA (General Services Administration). Alternate path analysis and design guidelines for progressive collapse resistance. Washington, DC; 2013.
[10] DOD (Department of Defense). Design of structures to resist progressive collapse.

Unified Facilities Criteria, UFC 4-023-03. Washington, DC; 2016.
[11] ACI (American Concrete Institute). Building code requirements for structural concrete and commentary, Farmington Hills; 2014.
[12] Yi WJ, He QF, Xiao Y, Kunnath SK. Experimental study on progressive collapse-resistant behavior of reinforced concrete frame structures. ACI Struct J 2008;105(4):433–9.
[13] Nimse RB, Joshi DD, Patel PV. Behavior of wet precast beam column connections under progressive collapse scenario: an experimental study. Adv Struct Eng 2014;6:149–59.
[14] Nimse RB, Joshi DD, Patel PV. Experimental study on precast beam column connections constructed using RC corbel and steel billet under progressive collapse scenario. In: Proceedings of Structures Congress. Reston, VA; ASCE; 2015.
[15] Tohidi M, Yang J, Baniotopoulos C. Numerical evaluations of codified design methods for progressive collapse resistance of precast concrete cross wall structures. Eng Struct 2014;76:177–86.
[16] Main JA, Bao YH, Lew HS, Sadek F, Chiatiro VP, Robert SD, Torres JO. An experimental and computational study of precast concrete moment frames under a column removal scenario. NIST TN-1886:1-56; 2015.
[17] Kang SB, Tan KH. Behavior of precast concrete beam-column sub-assemblages subject to column removal. Eng Struct 2015;93:95–6.
[18] Klasila E. Managing the progressive collapse of a corner of an office building built from precast concrete elements; 2016.
[19] Kang SB, Tan KH. Progressive collapse resistance of precast concrete frames with discontinuous reinforcement in the joint. ASCE J Struct Eng 2017;143(9):-1-1.
[20] Elsanadedy HM, Almusallam TH, Al-Salloum YA, Abbas H. Investigation of precast RC beam-column assemblies under column-loss scenario. Constr Build Mater 2017;142:552–71.
[21] Qian K, Li B. Performance of precast concrete substructures with dry connections to resist progressive collapse. ASCE J Perform Constr Facil 2018;32(2):04018005-1-14.
[22] Feng DC, Wu G, Lu Y. Numerical investigation on the progressive collapse behaviour of precast reinforced concrete frame subassemblages. ASCE. J Perform Constr Facil 2018:04018027.
[23] Lin KQ, Lu XZ, Li Y, Guan H. Experimental study of a novel multi-hazard resistant prefabricated concrete frame structure. Soil Dyn Earthquake Eng 2019;119:390–407.
[24] Spencer EQ, Clay JN, Corey TF. A non-emulative moment connection for progressive collapse resistance in precast concrete building frames. Eng Struct 2019;179:174–88.
[25] Bournas DA, Negro P, Molina FJ. Pseudodynamic tests on a full-scale 3-storey precast concrete building: behavior of the mechanical connections and floor diaphragms. Eng Struct 2013;57:609–27.
[26] Kataoka MN, Ferreira MA, Debs AL. Nonlinear FE analysis of slab-beam-column connection in precast concrete structures. Eng Struct 2017;143:306–15.
[27] Ren PQ, Li Y, Lu XZ, Guan H, Zhou YL. Experimental investigation of progressive collapse resistance of one-way reinforced concrete beam-slab substructures under a middle-column-removal scenario. Eng Struct 2016;118:28–40.
[28] Lu XZ, Lin KQ, Li Y, Guan H, Ren PQ, Zhou YL. Experimental investigation of RC beam-slab substructures against progressive collapse subject to an edge-column-removal scenario. Eng Struct 2017;2017(179):91–103.
[29] Qian K, Weng YH, Li B. Impact of two columns missing on dynamic response of RC flat slab structures. Eng Struct 2018;177:598–615.
[30] Qian K, Li B. Performance of precast concrete substructures with dry connections to resist progressive collapse. J Perform Constr Facil 2018;32(2):04018005.
[31] Qian K, Li B. Investigation into resilience of precast concrete floors against progressive collapse. ACI Struct J 2019;116(2):171–82.
[32] MHURDOC (Ministry of Housing and Urban-Rural Development of China). Code for design of concrete structures (GB 50010-2010), Beijing: China Architecture and Building Press; 2010 [in Chinese].
[33] MHURDOC (Ministry of Housing and Urban-Rural Development of China). Code for seismic design of building (GB 50011-2010), Beijing: China Architecture and Building Press; 2010 [in Chinese].
[34] Lu HS, Zhao FX. Site coefficients suitable to China site category. Acta Seismol Sin 2007;29(1):67–76.
[35] Vidjeapriya R, Jaya KP. Experimental study on two simple mechanical precast beam-column connections under reverse cyclic loading. ASCE J Perform Constr Facil 2013;27(4):402–14.
[36] Fan JY, Yuan YX. On the quadratic convergence of the Levenberg-Marquardt method without nonsingularity assumption. Computing 2005;74(1):23–39.
[37] Othman H, Marzouk H. Finite-Element analysis of reinforced concrete plates subjected to repeated impact loads. ASCE J Struct Eng 2017;143:04017120.
[38] Wriggers P. Computational contact mechanics. Berlin: Springer; 2006.
[39] Kwak H-G, Gang H. An improved criterion to minimize FE mesh-dependency in concrete structures under high strain rate conditions. Int J Impact Eng 2015;86:84–95.
[40] Genikomsou AS, Polak MA. Finite element analysis of punching shear of concrete slabs using damaged plasticity model in ABAQUS. Eng Struct 2015;98:38–48.